Journal of Quantitative Spectroscopy & Radiative Transfer 109 (2008) 770–788

Journal of Quantitative Spectroscopy & Radiative Transfer

www.elsevier.com/locate/jqsrt

Exact solution for the scattering and absorption properties of sphere clusters on a plane surface

Daniel W. Mackowski*

Mechanical Engineering Department, Auburn University, AL 36849, USA

Received 16 November 2006; received in revised form 22 August 2007; accepted 23 August 2007

Abstract

A formulation and computational scheme are presented for predicting the scattering and absorption cross-sections, and the scattering matrix elements, of clusters of non-intersecting spheres that are lying on or above an infinite plane surface and exposed to plane-wave radiation. The formulation provides an exact solution to Maxwell's equations and the associated boundary conditions on the spheres and the plane surface, and is applicable for arbitrary refractive indices for the spheres and the surface. A simplified strategy is presented for the calculation of the surface reflection matrix, which transforms the reflected scattered field from one sphere into a regular vector spherical harmonic expansion centered about another sphere. The calculation results are presented for the clusters of one, two, and four polystyrene spheres, with size parameters of one and 10, lying on a silicon substrate, and are compared with the predictions from the normal incidence approximation (NIA) in which the reflectance of the surface is assumed constant at the normal incidence value. The results show that the accuracy of the NIA is highly dependent on the extent of the sphere cluster, the angle of incidence, and the particular quantity (cross-sections, scattering matrix elements) under examination.

1. Introduction

The objective of this paper is on developing an exact theory—and a corresponding numerical calculation scheme—for predicting the scattering properties of the sphere clusters that are lying on a flat surface. The ability to quantify such properties has relevance in a number of fields and applications, i.e., detection of particles on semiconductor chips, the modeling of reflectance by pigment particle layers, assessing the effects of soot or mineral particle deposits on the absorptivity of ice, and so on. The problem, in itself, is also intrinsically interesting and challenging from a mathematical point of view, because it requires the matching of the boundary conditions on geometrically distinct classes of surfaces: the sphere and the plane.

Much previous work has been performed and reported on the prediction of scattering by a single sphere on a flat yet not-perfectly reflecting surface. A key aspect of the problem is the representation, in a spherical harmonic basis, of the electric field produced by the reflection of an outgoing (i.e., scattered) wave, i.e., the scattered–reflected field. Bobbert and Vlieger [1] utilized an integral representation of the outgoing vector

*Tel.: +1 334 844 3334; fax: +1 334 844 3307.
E-mail address: dmckwski@eng.auburn.edu

0022-4073/$ - see front matter © 2007 Elsevier Ltd. All rights reserved.
doi:10.1016/j.jqsrt.2007.08.024

harmonic to develop a comprehensive exact solution to Maxwell's time-harmonic equations for the sphere/surface system. However, the evaluation of the sphere–surface interaction terms—which generate a matrix relationship between the multipole orders of the outgoing harmonic and the regular harmonic expansion representing the reflected wave—requires the numerical integration of a product of rotational and complex exponential functions over the complex domain for each coupled multipole pair.

This feature of the problem has made the exact solution somewhat inaccessible, and has led subsequent teams—most notably the work of Videen et al.—to develop approximate solutions which are based on representing the reflected field as that produced by an 'image' source [2,3]. The rationale of this approach, referred to here as the normal incidence approximation (NIA), is that the sphere will interact primarily with the scattered radiation that is reflected at the near-normal incidence, and for this case the parallel and the perpendicular Fresnel reflection coefficients of the surface can be assumed to be constant (i.e., independent of the incident direction) and equal.

More recently, Fucile et al. [4], and Wriedt and Doicu [5], re-visited the exact solution for a sphere adjacent to a surface and developed equivalent formulations that are more compact and amenable to numerical evaluation than that presented in Ref. [1]. Wriedt and Doicu also generalized the solution to an arbitrary-shaped scatterer via the T matrix representation of the scattered field. Their calculation results for spheres—which were limited to a maximum sphere size parameter of $ka \approx 3$, a single angle of incidence, and a single value of surface refractive index—suggested that the NIA was quite adequate in representing the distribution of the scattered intensity. Johnson, on the other hand, compared the NIA with the numerical solutions generated by Wojcik et al. [6], and concluded that considerable error in the NIA could occur for dielectric surfaces [7]. The same conclusion regarding the NIA approximation was reached by Fucile et al. [4].

The current paper is concerned with multiple, mutually interacting spheres on a surface. For this case the NIA would be expected to be of more questionable status than for a single sphere, because the scattered radiation from one sphere will reflect off the surface to the other spheres at angles that are far from normal. In recognition of this, the paper will utilize the exact formulation of Wriedt and Doicu [5] to represent the surface interaction among the spheres. Fortunately, for this author, most of the heavy mathematical lifting needed for the model has been performed in Ref. [5], and extension to the multiple spheres case will be relatively straightforward. Such an extension has been presented by Denti et al. [8], who based their formulation on the assumption that the scattered–reflected field produced by a sphere, for a plane surface with arbitrary reflection properties, can be represented as a single outgoing vector spherical harmonic (VSH) expansion centered about the image point of the sphere [4]. The interaction of the scattered–reflected field with the neighboring spheres could then be computed using the translation theorems for the outgoing waves. However, it will be demonstrated here that a single-origin, VSH expansion is incapable of entirely representing the scattered–reflected field at all the points above the surface. Because of this, calculation of the scattered–reflected interactions among each sphere pair must begin with the fundamental integral relations for the spherical waves reflecting from plane surfaces as applied to the specific geometrical configuration for the pair. A key objective of the paper is to make the evaluation of these interaction terms—which unavoidably involves numerical quadrature—more tractable, and a scheme is presented which minimizes the computational overhead in this procedure.

2. Formulation

2.1. Configuration

The situation under examination is illustrated in Fig. 1. The system consists of N_S spheres, each with a radius a_i, refractive index m_i, and a position $\mathbf{r}_i = (x_i, y_i, z_i)$. The surface, characterized by a refractive index m_b, is located at $z = 0$ and the outward normal points in the $+z$ direction. A linearly polarized plane wave, of wavelength λ, is incident on the surface with a propagation direction defined by $\theta = \beta_i$ and $\phi = \alpha_i$. It is implied that $\beta_i < \pi/2$, i.e., the incident wave originates from the space above the plane. What is sought from the analysis, in the most general sense, is a complete and exact description of the electric field above the surface. More specifically, we wish to predict the absorption and scattering cross-sections of the individual spheres and the far-field scattering pattern.

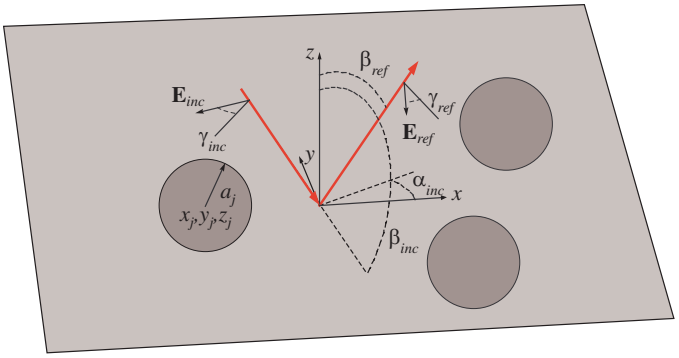

Fig. 1. The coordinate system.

The basic approach will involve a superposition solution to Maxwell's equations. Above the surface and exterior to the spheres the field will be represented by four basic components, being (1) the direct incident plane wave and (2) the scattered waves originating from the spheres, along with (3) the plane wave that is reflected off of the surface and (4) scattered waves that reflect off of the surface. The two components involving the scattered waves can be split further into contributions from the individual spheres, so that

$$\mathbf{E} = \mathbf{E}_{0,d} + \mathbf{E}_{0,r} + \sum_{j=1}^{N_S} (\mathbf{E}_{sd,j} + \mathbf{E}_{sr,j}) \tag{1}$$

in which $\mathbf{E}_{sd,j}$ and $\mathbf{E}_{sr,j}$ denote the direct and the reflected components of the scattered field due to sphere j.

The direct scattered fields can be represented by the outgoing VSH expansions, centered about the origin of each sphere.

$$\mathbf{E}_{sd,j} = \sum_{n=1}^{N_{O,j}} \sum_{m=-n}^{n} \sum_{p=1}^{2} a^j_{mnp} \mathbf{N}^{(3)}_{mnp}(\mathbf{r} - \mathbf{r}_j) \tag{2}$$

in which $\mathbf{N}^{(3)}_{mnp}$ is an outgoing VSH of order n, degree m, and mode p (= 1 for TM, 2 for TE), and $N_{O,j}$ denotes the truncation limit of the expansion. The VSH functions are defined in the Appendix. Determination of the scattered field expansion coefficients a^j is the objective of the problem.

The direct incident field, which is taken to have unit amplitude, can be represented by a regular VSH expansion about the target coordinate origin:

$$\mathbf{E}_{0,d} = (\hat{\mathbf{e}}_{\parallel} \cos\gamma_i + \hat{\mathbf{e}}_{\perp} \sin\gamma_i) \mathrm{e}^{\mathrm{i}\mathbf{k}_i \cdot \mathbf{r}} = \sum_{n=1}^{n} \sum_{m=-n}^{n} \sum_{p=1}^{2} p_{mnp} \mathbf{N}^{(1)}_{mnp}(\mathbf{r}) \tag{3}$$

with

$$p_{mnp} = -4\mathrm{i}^{n+1} \left(\tau_{mnp}(\cos\beta_i) \cos\gamma_i - \mathrm{i}\tau_{mn3-p}(\cos\beta_i) \sin\gamma_i \right) \mathrm{e}^{-\mathrm{i}m\alpha_i}. \tag{4}$$

In the above, γ_i denotes the angle between the incident electric vector and the plane formed by the propagation directions of the incident and the reflected fields; $\gamma = 0$ and $\pi/2$ correspond to the electric vector parallel and perpendicular to this plane. The angular functions τ_{mnp} are defined by

$$\tau_{mn1}(x) = -(1-x^2)^{1/2} \left(\frac{2n+1}{n(n+1)} \frac{(n-m)!}{(n+m)!} \right)^{1/2} \frac{\mathrm{d}P^m_n(x)}{\mathrm{d}x}, \tag{5}$$

$$\tau_{mn2}(x) = m(1-x^2)^{-1/2} \left(\frac{2n+1}{n(n+1)} \frac{(n-m)!}{(n+m)!} \right)^{1/2} P^m_n(x). \tag{6}$$

Note that the convention $3-p$ in Eq. (4) is used to switch the mode from one to another.

The reflected plane wave $\mathbf{E}_{0,r}$ will be given by a regular VSH expansion, centered about the target origin, that is similar to Eq. (3):

$$\mathbf{E}_{0,r} = (\hat{\mathbf{e}}_{\parallel} \cos\gamma_r r_{\parallel}(\cos\beta_r) + \hat{\mathbf{e}}_{\perp} \sin\gamma_r r_{\perp}(\cos\beta_r))\mathrm{e}^{\mathrm{i}\mathbf{k}_r\cdot\mathbf{r}} = \sum_{n=1}^{n}\sum_{m=-n}^{n}\sum_{p=1}^{2} g_{mnp}\mathbf{N}^{(1)}_{mnp}(\mathbf{r}) \tag{7}$$

in which $r_{\parallel}$ and $r_{\perp}$ are the reflection coefficients for the surface [9]:

$$r_{\parallel}(\cos\beta_r) = -\frac{m_b\cos\beta_r - \cos\beta_{\mathrm{t}}}{m_b\cos\beta_r + \cos\beta_{\mathrm{t}}}, \tag{8}$$

$$r_{\parallel}(\cos\beta_r) = \frac{\cos\beta_r - m_b\cos\beta_{\mathrm{t}}}{\cos\beta_r + m_b\cos\beta_{\mathrm{t}}} \tag{9}$$

with $\cos\beta_{\mathrm{t}}$ being the cosine of the transmission angle:

$$\cos\beta_{\mathrm{t}} = \left(1 - \left[\frac{1-\cos^2\beta_r}{m_b^2}\right]\right)^{1/2}. \tag{10}$$

Note that the parallel reflection coefficient $r_{\parallel}$ used here is the negative of that employed in Ref. [5]. Since the origin of the expansion is on the surface there is no need to account for the phase shift between the incident and the reflected fields. The reflected expansion coefficients then appear as

$$g_{mnp} = -4\mathrm{i}^{n+1}(\tau_{mnp}(\cos\beta_r)\cos\gamma_r r_{\parallel}(\cos\beta_r) - \mathrm{i}\tau_{mn3-p}(\cos\beta_r)\sin\gamma_r r_{\perp}(\cos\beta_r))\mathrm{e}^{-\mathrm{i}m\alpha_r}. \tag{11}$$

Following the usual convention for characterizing reflection from a surface, the reflection angle $\beta_r = \pi - \beta_i$ will be used as the parameter which characterizes the incident field. In this sense normal incidence corresponds to $\beta_r = 0$. Furthermore, $\alpha_i = \alpha_r$ and $\gamma_i = \pi - \gamma_r$. Using

$$\tau_{mnp}(-x) = (-1)^{m+n+p}\tau_{mnp}(x), \tag{12}$$

the incident field coefficients in Eq. (4) are reformulated as

$$p_{mnp} = 4(-1)^{m+n+p}\mathrm{i}^{n+1}(\tau_{mnp}(\cos\beta_r)\cos\gamma_r - \mathrm{i}\tau_{mn3-p}(\cos\beta_r)\sin\gamma_r)\mathrm{e}^{-\mathrm{i}m\alpha_r}. \tag{13}$$

To formulate the sphere/surface interaction equations it will be necessary to expand the incident and the reflected fields about each of the spheres in the cluster. That is, a regular VSH expansion is sought for the incident and the reflected fields in the form of Eq. (2), with the regular harmonics centered about the origin of sphere j. The coefficients in these expansion can be obtained by two methods. The first is to multiply the p and g coefficients by the phase shift that occurs between the target origin and the origin of sphere j. Since the incident field propagates in the $\theta = \pi - \beta_r$, $\phi = \alpha_r$ direction, and the reflected in the $\theta = \beta_r$, $\phi = \alpha_r$ direction, the incident and the reflected coefficients about sphere j will be

$$p^j_{mnp} = p_{mnp}\exp[\mathrm{i}k[(x_j\cos\alpha_r + y_j\sin\alpha_r)\sin\beta_r - z_j\cos\beta_r]], \tag{14}$$

$$g^j_{mnp} = g_{mnp}\exp[\mathrm{i}k[(x_j\cos\alpha_r + y_j\sin\alpha_r)\sin\beta_r + z_j\cos\beta_r]]. \tag{15}$$

A second method is to apply the addition theorem for VSH to translate the incident and the reflected coefficients to the various origins. For regular VSH, the addition theorem takes the form

$$\mathbf{N}^{(1)}_{mnp}(\mathbf{r}) = \sum_{l}\sum_{k=-l}^{l}\sum_{q=1}^{2} J^{j-0}_{klq\,mnp}\mathbf{N}^{(1)}_{klq}(\mathbf{r} - \mathbf{r}_j). \tag{16}$$

The translation matrix J^{j-0} depends solely on the distance and the direction of the translation from origin 0 (the cluster origin) to j; formulas are given in the Appendix. The number of orders l required for convergence of the expansion will depend on the distance of the translation; in general, $J^{j-0}_{klq\,mnp} \to 0$ for $|n-l| \gg k|\mathbf{r}_j|$. By the application of the above formula to Eqs. (3) and (7), the translated incident and reflected field coefficients

are obtained by the same general formula:

$$p^j_{mnp} = \sum_l \sum_{k=-l}^{l} \sum_{q=1}^{2} J^{j-0}_{mnp\,klq} p_{klq}, \tag{17}$$

$$g^j_{mnp} = \sum_l \sum_{k=-l}^{l} \sum_{q=1}^{2} J^{j-0}_{mnp\,klq} g_{klq}. \tag{18}$$

2.2. The scattered and reflected field

Outlined here is the formulation developed by Wriedt and Doicu for obtaining a regular VSH expansion for the field produced by the plane surface reflection of the outgoing scattered waves from the spheres [5]. For all points $\mathbf{r}-\mathbf{r}_j$ such that $z-z_j<0$, an outgoing VSH can be obtained via

$$\mathbf{N}^{(3)}_{mnp}(\mathbf{r}-\mathbf{r}_j) = -\frac{(-\mathrm{i})^{n+1}}{2\pi}\int_0^{2\pi}\int_{\pi/2+\mathrm{i}\infty}^{\pi} (\tau_{mnp}(\cos\beta)\hat{\beta} + \mathrm{i}\tau_{mn3-p}(\cos\beta)\hat{\alpha})\mathrm{e}^{\mathrm{i}m\alpha}\mathrm{e}^{\mathrm{i}\mathbf{k}\cdot(\mathbf{r}-\mathbf{r}_j)}\,\mathrm{d}\Omega \tag{19}$$

in which $\mathrm{d}\Omega = \sin\beta\,\mathrm{d}\beta\,\mathrm{d}\alpha$, $\hat{\beta}$ and $\hat{\alpha}$ correspond to unit vectors in the β and α directions, and

$$\mathbf{k}\cdot(\mathbf{r}-\mathbf{r}_j) = k[((x-x_j)\cos\alpha + (y-y_j)\sin\alpha)\sin\beta + (z-z_j)\cos\beta]. \tag{20}$$

By a comparison with Eq. (4), Eq. (19) can be viewed as a representation of the outgoing VSH by a plane-wave spectrum, although the spectrum of propagation directions β covers both the real and imaginary (i.e., evanescent) angles. Nevertheless, along the surface at $z=0$, each plane-wave component—real and imaginary—will be reflected according to the Fresnel relations. By using the same relations employed in the formulation of Eq. (11), the reflected field produced by the outgoing VSH will be

$$\begin{aligned}\mathbf{N}^{(3)}_{mnp}(\mathbf{r}-\mathbf{r}_j)|_r = (-1)^{m+n+p}\frac{(-\mathrm{i})^{n+1}}{2\pi}\int_0^{2\pi}\int_0^{\pi/2-\mathrm{i}\infty} &(\tau_{mnp}(\cos\beta)r_{\parallel}(\cos\beta)\hat{\beta}\\ &+ \mathrm{i}\tau_{mn3-p}(\cos\beta)r_{\perp}(\cos\beta)\hat{\alpha})\mathrm{e}^{\mathrm{i}m\alpha}\mathrm{e}^{\mathrm{i}\mathbf{k}\cdot(\mathbf{r}-\mathbf{r}_j)}\mathrm{e}^{2\mathrm{i}kz_j\cos\beta}\,\mathrm{d}\Omega.\end{aligned} \tag{21}$$

Note that the integration now occurs for the upwards directions. The range of convergence of the formula is $z> -z_j$; this formally includes all of the region of interest yet this limit will become relevant when Eq. (21) is cast as an expansion of regular VSH.

As per Eq. (3), the phase factor involving $\mathbf{k}\cdot(\mathbf{r}-\mathbf{r}_j)$ can be cast into a plane-wave VSH expansion centered about a second origin i with the parallel and perpendicular components equivalent to $\hat{\beta}$ and $\hat{\alpha}$. That is,

$$\begin{aligned}(\hat{\beta},\hat{\alpha})\exp(\mathbf{k}\cdot(\mathbf{r}-\mathbf{r}_j)) &= (\hat{\beta},\hat{\alpha})\exp(\mathbf{k}\cdot(\mathbf{r}-\mathbf{r}_i))\exp(\mathbf{k}\cdot(\mathbf{r}_i-\mathbf{r}_j))\\ &= -4\mathrm{e}^{(\mathbf{k}\cdot(\mathbf{r}_i-\mathbf{r}_j))}\sum_{l=1}\sum_{k=-l}^{l}\sum_{q=1}^{2}\mathrm{i}^{l+1}(\tau_{klq}(\cos\beta), -\mathrm{i}\tau_{kl3-q}(\cos\beta))\mathrm{e}^{-\mathrm{i}k\alpha}\mathbf{N}^{(1)}_{klq}(\mathbf{r}-\mathbf{r}_i).\end{aligned} \tag{22}$$

Combining this with Eq. (21) results in

$$\begin{aligned}\mathbf{N}^{(3)}_{mnp}(\mathbf{r}-\mathbf{r}_j)|_r = -\frac{2}{\pi}(-1)^{m+n+p}\sum_{l=1}\sum_{k=-l}^{l}\sum_{q=1}^{2}\mathbf{N}^{(1)}_{klq}(\mathbf{r}-\mathbf{r}_i)(\mathrm{i})^{l-n}\int_0^{2\pi}\int_0^{\pi/2-\mathrm{i}\infty} &(\tau_{mnp}(\cos\beta)r_{\parallel}(\cos\beta)\tau_{klq}(\cos\beta)\\ &+ \tau_{mn3-p}(\cos\beta)r_{\perp}(\cos\beta)\tau_{kl3-q}(\cos\beta))\mathrm{e}^{\mathrm{i}(m-k)\alpha}\mathrm{e}^{2\mathrm{i}kz_j\cos\beta}\mathrm{e}^{\mathrm{i}\mathbf{k}\cdot(\mathbf{r}_i-\mathbf{r}_j)}\sin\beta\,\mathrm{d}\beta\,\mathrm{d}\alpha.\end{aligned} \tag{23}$$

The above formula can be condensed into a matrix transformation that gives the regular VSH expansion, about origin $\mathbf{r}_i$, produced by the reflection of the outgoing VSH centered at $\mathbf{r}_j$:

$$\mathbf{N}^{(3)}_{mnp}(\mathbf{r}-\mathbf{r}_j)|_r = \sum_{l=1}\sum_{k=-l}^{l}\sum_{q=1}^{2} R^{i-j}_{klq\,mnp}\mathbf{N}^{(1)}_{klq}(\mathbf{r}-\mathbf{r}_i). \tag{24}$$

The formula for the coefficients of the reflection matrix R^{i-j} can be simplified considerably from that appearing in Eq. (23). The integration over α can be performed analytically via

$$\int_0^{2\pi} \exp[\mathrm{i}((m-k)\alpha + k[(x_i-x_j)\cos\alpha + (y_i-y_j)\sin\alpha]\sin\beta)]\,\mathrm{d}\alpha$$
$$= \int_0^{2\pi} \exp[\mathrm{i}((m-k)\alpha + k\rho_{ij}\sin\beta\cos(\alpha-\phi_{ij}))]\,\mathrm{d}\alpha = 2\pi\mathrm{i}^{|m-k|}J_{|m-k|}(k\rho_{ij}\sin\beta)\mathrm{e}^{\mathrm{i}(m-k)\phi_{ij}} \tag{25}$$

in which J_v is the ordinary Bessel function of order v, and

$$\rho_{ij} = [(x_i-x_j)^2 + (y_i-y_j)^2]^{1/2}, \quad \mathrm{e}^{\mathrm{i}\phi_{ij}} = \frac{(x_i-x_j)+\mathrm{i}(y_i-y_j)}{\rho_{ij}}. \tag{26}$$

The products involving the angular functions $\tau_{mnp}\tau_{klq}$ can also be linearized. The angular functions are related to the general spherical functions $\mathscr{D}^{(n)}_{mk}$ (defined in the Appendix) by

$$\tau_{mnp}(x) = -\tfrac{1}{4}(2n+1)^{1/2}((-1)^p\mathscr{D}^{(n)}_{-m1}(x) + \mathscr{D}^{(n)}_{-m-1}(x)). \tag{27}$$

The product of two spherical functions, each with the same argument, can be expanded into

$$\mathscr{D}^{(n)}_{-ms}(x)\mathscr{D}^{(l)}_{-kt}(x) = (-1)^{k+t}\sum_w C^w_{mn,-kl}C^w_{-sn,tl}\mathscr{D}^{(w)}_{k-ms-t}(x) \tag{28}$$

in which $C^w_{mn,\,kl}$ is shorthand for the Clebsch–Gordan coefficient $C(n,m;l,k;w,m+k)$ and the sum over w runs from $|n-l|$ to $n+l$. By using

$$C^w_{sn,-tl} = (-1)^{n+l+w}C^w_{-sn,\,tl} \tag{29}$$

and introducing the integrals

$$Q^{i-j}_{vwu} = \mathrm{i}^{|v|}\int_{0+\mathrm{i}\infty}^{1}(r_\parallel(x) + \mathrm{i}^u r_\perp(x))\mathscr{D}^{(w)}_{vu}(x)J_{|v|}(\rho_{ij}(1-x^2)^{1/2})\mathrm{e}^{\mathrm{i}k(z_i+z_j)x}\,\mathrm{d}x, \tag{30}$$

the matrix elements can be expressed as

$$R^{i-j}_{klq\,mnp} = \frac{1}{4}(-1)^{m+k+n+p}\mathrm{i}^{l-n}[(2n+1)(2l+1)]^{1/2}\mathrm{e}^{\mathrm{i}(m-k)\phi_{ij}}$$
$$\times\sum_w C^w_{mn,\,-kl}[((-1)^{p+q+n+l+w}+1)C^w_{1n,-1l}Q^{i-j}_{k-m\,w0}$$
$$+(-1)^q C^w_{1n,1l}((-1)^{p+q+n+l+w}Q^{i-j}_{k-m\,w2} + Q^{i-j}_{k-m\,w-2})]. \tag{31}$$

With the exception of a perfectly reflecting surface, for which a simple image-based formula for the reflection matrix can be derived, evaluation of the elements of the reflection matrix will require numerical integration of the Q^{i-j}_{vwu} functions in Eq. (30). By linearizing the rotation function products, a result is obtained which minimizes the parameter space over which the integration must be performed, i.e., integration is performed for the vector elements $u=-2,0,2$, $w=|u|,|u|+1,\ldots,$ and $v=0,1,\ldots w$, with $Q_{-vwu}=(-1)^v Q_{vw-u}$, as opposed to integrating for each matrix element klq, mnp in Eq. (23). For a maximum order on n and l in Eq. (24) of $N_{\mathrm{O},j}$ and $N_{\mathrm{O},i}$, respectively, the maximum required order w for the Q_{vwu} functions will be $N_{\mathrm{O},j}+N_{\mathrm{O},i}$.

For the displacement between the arbitrary origins j and i, the reflection matrix has the symmetry property of

$$R^{i-j}_{klq\,mnp} = R^{i-j}_{-mnp\,-klq} = (-1)^{m+k}R^{j-i}_{klq\,mnp}. \tag{32}$$

The special case of self-interaction will have $Q^{j-j}_{vwu}=0$ for $v\neq 0$ and $R^{j-j}_{klq\,mnp}=0$ for $m\neq k$.

A generalized, adaptive Romberg algorithm is used to evaluate the integrals in Eq. (30), and the integration domain is split according to [10]

$$\int_{0+i\infty}^{1} f(x)\,\mathrm{d}x = \int_{0}^{1} f(x)\,\mathrm{d}x - \mathrm{i}\int_{0}^{\infty} f(i\,x)\,\mathrm{d}x. \tag{33}$$

2.2.1. Normal incidence approximation

Videen et al. developed an approximation for the reflection matrix by taking the Fresnel coefficients to be constant and equal to the normal incidence values, i.e., $r_\parallel = r_\perp = r_0$ [2]. By doing so, the scattered–reflected field from sphere j becomes equivalent to that produced by an image source at j_R, with the electric field modified by the reflectance r_0. The regular VSH expansion, centered about the sphere origin i, of the scattered–reflected field can then be obtained by the application of the addition theorem to the image field. The end result is

$$R^{i-j}_{klq\,mnp} \approx -(-1)^{m+n+p} r_0 H^{i-j_R}_{klq\,mnp} \tag{34}$$

in which H^{i-j_R} is a translation matrix which transforms, analogous to Eq. (16), an outgoing VSH at the origin of the image point j_R, with $\mathbf{r}_{j_R} = (x_j,\ y_j, -z_j)$, into a regular VSH expansion about origin i.

The single-sphere rationale for the NIA is based on a geometrical optics argument, in that the maximum reflection angle for the rays leaving one point on the sphere and striking another point *on the same sphere* will be 30°, and within this range the Fresnel coefficients for most surfaces are fairly constant. The sphere therefore 'sees' its reflection over a surface with a uniform reflectivity. On the mathematical side, the NIA will analytically result from the exact formula for the reflectance matrix for the condition $r_\parallel = r_\perp =$ constant [5,11].

2.2.2. Image source model

Fucile et al. made the assumption that the scattered–reflected field produced by a sphere, for a surface with arbitrary reflection properties, could be represented at all the points in the half space $z \geqslant 0$ by a single outgoing VSH expansion centered about the image point of the sphere [4]. That is, the model assumes that, for sphere j,

$$\mathbf{N}^{(3)}_{mnp}(\mathbf{r} - \mathbf{r}_j)|_r = \sum_{l=1}^{l} \sum_{k=-l}^{l} \sum_{q=1}^{2} F^{j}_{klq\,mnp} \mathbf{N}^{(3)}_{klq}(\mathbf{r} - \mathbf{r}_{j_R}). \tag{35}$$

Their approach to determining the expansion matrix F was to transform, via the addition theorem, the outgoing harmonics in Eq. (35) into an expansion of regular harmonics about the source sphere j, and then match the resulting formula with Eq. (24). This gives (in matrix form)

$$\mathbf{F}^{j} = (\mathbf{H}^{j-j_R})^{-1} \cdot \mathbf{R}^{j-j}. \tag{36}$$

This model represents a heuristic extension of the NIA to arbitrary surface properties. The main computational advantage of the model is that the reflection matrix R need only be calculated for each individual sphere (i.e., R^{j-j}), and the interactions among the neighboring spheres can be obtained from the application of the addition theorem via

$$\mathbf{R}^{i-j} = \mathbf{H}^{i-j_R} \cdot \mathbf{F}^{j}. \tag{37}$$

However, the image source model does not appear to be consistent with the exact formulas for the outgoing and the scattered–reflected VSH as given in Eqs. (19) and (21). Making use of the axial symmetry between the source (j) and the image (j_R) points, the image source model implies an expansion of the form

$$\begin{aligned} &-(-1)^{m+n+p}(\tau_{mnp}(\cos\beta) r_\parallel(\cos\beta)\hat{\beta} + \mathrm{i}\tau_{mn3-p}(\cos\beta) r_\perp(\cos\beta)\hat{\alpha}) \\ &\quad = \sum_{k,l,q} F_{klq\,mnp}(\tau_{klq}(\cos\beta)\hat{\beta} + \mathrm{i}\tau_{kl3-q}(\cos\beta)\hat{\alpha}). \end{aligned} \tag{38}$$

The $\tau(\cos\beta)$ functions have useful orthogonality properties which could be employed to determine F from the above expansion, yet these properties apply only to integration over the unit sphere, i.e., real β, whereas

Eq. (38) must hold for real as well as imaginary β. Conversely, neither side of Eq. (38) will converge when integrated over the complex half-sphere domain $\beta = (0, \pi/2 - i\infty)$. Because of this, the relationship in Eq. (38)—which is central to the validity of the image source model—cannot be established for the integration domain of β appearing in Eq. (21). This flaw will have no effect on the model when applied or the case of a single sphere on or near a surface, for which the self-interaction matrix, via Eqs. (36) and (37), will return the exact result, yet it will have bearing on the multiple sphere case.

A conclusion is that the scattered–reflected field, for arbitrary surface properties, cannot be represented *for all the points above the surface* as a single outgoing VSH expansion *centered about a single point*. That such is the case is not surprising when one considers that, in the most general sense, the scattered–reflected field must be equivalent to the radiation scattered from a collection of dipole sources that collectively represent the surface medium. An expansion of the form of Eq. (35) would be valid for radii $|\mathbf{r} - \mathbf{r}_j|$ that enclose all of the dipole sources—which is impossible except in the far field.

2.3. The interaction equations

The formulas for the reflected incident field (Eq. (7)) and the scattered–reflected field (Eq. (24)) can now be appended into the equations for electromagnetic wave interaction among multiple spheres. The interaction equations represent a generalization of a T matrix relationship for each sphere; in that the coefficients for the scattered field from the sphere, a^j_{mnp}, will be linearly related to the coefficients describing the net exciting field at the sphere. Note that the latter will be comprised of four components, being the direct and the reflected incident fields, the direct scattered fields from other spheres, and the reflected scattered field. The direct scattered field, from the neighboring spheres, can be cast in a regular VSH expansion about the origin of j by the application of the addition theorem, and the other three components have already been represented by regular VSH expansions in the previous formulas. Putting all together, the interaction equations will appear as

$$\frac{1}{\overline{a}^j_\mu} a^j_\mu - \sum_{\substack{i=1 \\ i\neq j}}^{N_S} \sum_\nu H^{j-i}_{\mu\nu} a^i_\nu - \sum_{i=1}^{N_S} \sum_\nu R^{j-i}_{\mu\nu} a^i_\nu = p^j_\mu + g^j_\mu. \tag{39}$$

In the above, Greek subscripts μ and ν are shorthand for degree/order/mode, i.e., $\mu \equiv (mnp)$. The quantity $\overline{a}^j_\mu \equiv \overline{a}^j_{np}$ is the T matrix coefficient for the sphere; these are typically referred to as the Lorenz–Mie coefficients although they are the negative of the commonly defined LM coefficients, e.g., Ref. [9].

For equal-sized spheres, and assuming that the truncation orders for the individual scattered field expansions are the same at N_O, Eq. (39) represents $2N_S N_O(N_O + 2)$ complex-valued equations for the set of scattering coefficients. The scattering and absorption properties of the spheres, for a specified incidence angle and polarization, can be obtained directly from the scattering coefficients via formulas presented in the next section.

2.4. Far-field scattering

In the far-field region the direct scattered field, from sphere j, is obtained using the asymptotic form of the outgoing VSH:

$$\mathbf{E}_{sd,j,\mathrm{ff}} = \frac{1}{ikr} e^{ik|\mathbf{r}-\mathbf{r}_j|} \sum_n \sum_{m=-n}^{n} \sum_{p=1}^{2} (-i)^{n+1} (\tau_{mnp}(\cos\theta)\hat{\mathbf{e}}_\theta + i\tau_{mn3-p}(\cos\theta)\hat{\mathbf{e}}_\phi) e^{im\phi} a^j_{mnp}. \tag{40}$$

The far-field scattered–reflected field from sphere j can be obtained from Eq. (21) in the limit of $k|\mathbf{r}| \gg n$ [3,5], and leads to the simple result

$$\begin{aligned} \mathbf{E}_{sr,j,\mathrm{ff}} = & -\frac{1}{ikr} e^{ik|\mathbf{r}-\mathbf{r}_{j_R}|} \sum_n \sum_{m=-n}^{n} \sum_{p=1}^{2} (-i)^{n+1} (\tau_{mnp}(\cos\theta) r_\parallel(\cos\theta)\hat{\mathbf{e}}_\theta \\ & + i\tau_{mn3-p}(\cos\theta) r_\perp(\cos\theta)\hat{\mathbf{e}}_\phi) e^{im\phi} (-1)^{m+n+p} a^j_{mnp}, \end{aligned} \tag{41}$$

where $\mathbf{r}_{j_R} = (x_j, y_j, -z_j)$ again refers to the location of the image source for sphere j.

In the far field, outgoing harmonics will obey the same translation formula in Eq. (16), and this formula can be used to shift Eqs. (40) and (41), which represent sources at the points $\mathbf{r}_j$ and $\mathbf{r}_{j_R}$, to expansions based on the target origin. By applying the property

$$J^{0-j_R}_{mnp\,klq} = (-1)^{m+n+p}(-1)^{k+l+q} J^{0-j}_{mnp\,klq} \tag{42}$$

the total (direct and reflected) scattered field from the entire ensemble can be cast as

$$\begin{aligned}\mathbf{E}_s = \frac{1}{\mathrm{i}k\,r}\mathrm{e}^{\mathrm{i}k\,r}\sum_n\sum_{m=-n}^{n}\sum_{p=1}^{2}(-\mathrm{i})^{n+1}(\tau_{mnp}(\cos\theta)(1-(-1)^{m+n+p}r_{\parallel}(\cos\theta))\hat{\mathbf{e}}_\theta \\ + \mathrm{i}\tau_{mn3-p}(\cos\theta)(1-(-1)^{m+n+p}r_{\perp}(\cos\theta))\hat{\mathbf{e}}_\phi)\mathrm{e}^{\mathrm{i}m\phi}a_{mnp}\end{aligned} \tag{43}$$

in which the total scattered field coefficients are obtained from

$$a_{mnp} = \sum_{j=1}^{N_S}\sum_{l=1}^{N_{O,j}}\sum_{k=-l}^{l}\sum_{q=1}^{2} J^{0-j}_{mnp\,klq}\,a^{j}_{klq}. \tag{44}$$

These results are consistent with the far-field formulation for multiple spheres on a surface developed by Denti et al. [8].

The usual scheme that is applied to an isolated particle will be used to define the amplitude and the scattering matrices of the sphere–surface system. The scattering plane is defined by the plane containing the direct incident and the scattering directions, and the amplitude matrix is obtained as the relationship between the incident and the scattered field components that are parallel and perpendicular to this plane. However, for the sphere–surface system it is most practical to retain the surface-normal-based polar coordinate system for mapping the amplitude and the scattering matrix, and to do this will require some geometric manipulations because the scattering plane will not, in general, contain the surface normal.

The value of γ_r, which denotes the polarization angle in Eqs. (4) and (11), that results in the incident electric vector parallel to the scattering plane will be given by

$$\tan\gamma_r = \frac{\sin\theta\sin(\alpha_r-\phi)}{\sin\theta(\sin(\alpha_r-\phi)-\cos\beta_r\cos(\alpha_r-\phi))-\cos\theta\sin\beta_r}. \tag{45}$$

The fact that γ_r—and, by an extension, the right-hand side to the interaction equations in Eq. (39)—depends on the scattering direction θ and ϕ would appear to imply that the equations would need to be solved anew to calculate the amplitude and the scattering matrices for each scattering direction. This, however, is not the case because the values of the incident field coefficients p^j_{mnp} and g^j_{mnp}, for an arbitrary value of γ_r, will be a linear combination of the coefficients evaluated for $\gamma_r = 0$ and $\pi/2$, i.e., for the incident field parallel and perpendicular to the surface normal. In this sense, define as $a_{mnp,1}$ and $a_{mnp,2}$ the total scattering coefficients that are calculated for a given value of β_r and α_r and for $\gamma_r = \pi/2$ and 0, respectively. The values of the scattering coefficients, for the incident field parallel and perpendicular to the scattering plane, will then be

$$a_{mnp,\parallel} = a_{mnp,2}\cos\gamma_r + a_{mnp,1}\sin\gamma_r, \tag{46}$$

$$a_{mnp,\perp} = -a_{mnp,2}\sin\gamma_r + a_{mnp,1}\cos\gamma_r. \tag{47}$$

With regard to the scattered field, the components that are parallel and perpendicular to the scattering plane will be given by

$$\mathbf{E}_{s,\parallel} = \mathbf{E}_{s,\theta}\cos\gamma_s + \mathbf{E}_{s,\phi}\sin\gamma_s, \tag{48}$$

$$\mathbf{E}_{s,\perp} = -\mathbf{E}_{s,\theta}\sin\gamma_s + \mathbf{E}_{s,\phi}\cos\gamma_s \tag{49}$$

with the angle γ_s given by

$$\tan\gamma_s = \frac{\sin\beta\sin(\alpha_r-\phi)}{\sin\beta(\sin(\alpha_r-\phi)+\cos\theta\cos(\alpha_r-\phi))+\cos\beta_r\sin\theta}. \tag{50}$$

Putting it all together, the amplitude matrix elements are obtained from the following formulas:

$$\Pi_{mnp,1} \equiv \mathrm{i}(-\mathrm{i})^{n+1}\tau_{mnp}(\cos\theta)(1+(-1)^{m+n+p}r_{\perp}(\cos\theta))\mathrm{e}^{\mathrm{i}m\phi}, \tag{51}$$

$$\Pi_{mnp,2} \equiv (-\mathrm{i})^{n+1}\tau_{mnp}(\cos\theta)(1-(-1)^{m+n+p}r_{\parallel}(\cos\theta))\mathrm{e}^{\mathrm{i}m\phi}, \tag{52}$$

$$S_1 = \sum_n \sum_{m=-n}^{n} \sum_{p=1}^{2} (-\Pi_{mnp,2}\sin\gamma_s + \Pi_{mn3-p,1}\cos\gamma_s), a_{mnp\perp}, \tag{53}$$

$$S_2 = \sum_n \sum_{m=-n}^{n} \sum_{p=1}^{2} (\Pi_{mnp,2}\cos\gamma_s + \Pi_{mn3-p,1}\sin\gamma_s), a_{mnp\parallel}, \tag{54}$$

$$S_3 = \sum_n \sum_{m=-n}^{n} \sum_{p=1}^{2} (\Pi_{mnp,2}\cos\gamma_s + \Pi_{mn3-p,1}\sin\gamma_s), a_{mnp\perp}, \tag{55}$$

$$S_4 = \sum_n \sum_{m=-n}^{n} \sum_{p=1}^{2} (-\Pi_{mnp,2}\sin\gamma_s + \Pi_{mn3-p,1}\cos\gamma_s), a_{mnp\parallel}. \tag{56}$$

Given the amplitude matrix, the elements of the scattering matrix can be obtained from the standard formulas [9]. In particular, the scattered intensity for the incident radiation of the irradiance I_0 will be

$$I_s(\theta,\phi) = I_0 S_{11} = \frac{1}{2} I_0 \sum_{i=1}^{4} |S_i|^2. \tag{57}$$

2.5. Cross-sections

One of the most relevant goals of the current investigation is to formulate how the interactions between the spheres and the surface affect energy transfer to the spheres and to the surface. Such an analysis can be performed by the calculation of the appropriate cross-sections of the cluster and comparison to the isolated particle values. However, it is important to note that the present sphere/surface situation offers multiple ways in which the particle cross-sections can be defined. In general, a cross-section is obtained as the ratio of the power—either scattered or extinction—crossing a (usually closed) surface to the incident irradiance I_0. In the present case, the surface can either conform to the sphere surfaces—which results in the traditional aerosol definitions of cross-sections—or over a hemisphere enclosing the cluster and extending laterally along the surface to infinity. As was noted by Johnson [7], the latter definition is, in many respects, more relevant with regard to measurable quantities.

The hemispherical (or surface-based) extinction cross-section is defined so that $I_0 C_{\mathrm{ext,S}}$ is the rate at which the cluster removes energy from the beam in the reflected (or forward) direction of $\theta = \beta_r$, $\phi = \alpha_r$. This quantity is predicted via the optical theorem, in which the reflected beam is represented by the transverse plane wave of Eq. (7) [7]. For perpendicular and parallel incident field states, the cross-sections are

$$C_{\mathrm{ext,S},1} = -\frac{4\pi}{k^2}\,\mathrm{Re}(r_{\perp}^{*}(\cos\beta_r)S_1(\cos\beta_r,\alpha_r)), \tag{58}$$

$$C_{\mathrm{ext,S},2} = -\frac{4\pi}{k^2}\,\mathrm{Re}(r_{\parallel}^{*}(\cos\beta_r)S_2(\cos\beta_r,\alpha_r)). \tag{59}$$

The extinction cross-section for the unpolarized incident radiation will be the average of the one and two values.

Analogous to the surface extinction cross-section, a surface scattering cross-section can be defined so that $I_0 C_{\mathrm{sca}}$ is the rate at which the cluster scatters energy from the surface. For the unpolarized incident radiation,

the cross-section is obtained from

$$C_{\mathrm{sca,S}} = \frac{\pi}{k^2}\int_0^{2\pi}\int_0^{\pi/2} S_{11}(\theta,\phi)\sin\theta\,\mathrm{d}\theta\,\mathrm{d}\phi. \tag{60}$$

Except for the limiting case of perfect surface reflection, the quadrature methods must be used to perform the integration over θ. Since $I_0 C_{\mathrm{sca}}$ describes the scattered energy leaving the surface, it follows from an energy balance that $I_0 C_{\mathrm{abs,S}} = I_0(C_{\mathrm{ext,S}} - C_{\mathrm{sca,S}})$ describes the net change in the energy transfer into the surface due to the presence of the cluster. The surface absorption cross-section accounts for both the absorption by the cluster and scattered radiation from the cluster that is absorbed by the surface. And unlike the corresponding absorption cross-section for the isolated particle, the surface absorption cross-section can be positive or negative—indicating that the cluster either enhances or decreases the absorptivity of the surface.

Indeed, an effective surface absorptivity can be defined; say particles (single spheres or clusters) are lying on the surface with a surface number density of N'' (particles/unit area), and that the particles are spaced sufficiently far apart so that they can be assumed to scatter independently. The absorbed flux of energy by the surface would be

$$q'' = I_0[(1-|r|^2)\cos\beta_r + N''\langle C_{\mathrm{abs,S}}\rangle], \tag{61}$$

where $\langle C_{\mathrm{abs,S}}\rangle$ denotes the ensemble-averaged surface absorption cross-section. By defining an efficiency factor via $C_{\mathrm{abs,S}} = \pi a_{\mathrm{C}}^2 Q_{\mathrm{abs,S}}$, where πa_{C}^2 is the projected area of the particle in the surface-normal direction, and denoting the particle/surface area fraction as $f_A = N''\pi a_{\mathrm{C}}^2$, the effective absorptivity of the surface is

$$\alpha_{\mathrm{eff}} = \frac{q''}{I_0\cos\beta_r} = 1 - |r|^2 + \frac{f_A\langle Q_{\mathrm{abs,S}}\rangle}{\cos\beta_r}. \tag{62}$$

As mentioned above, the surface-based cross-sections represent the quantities which are accessible by measurement of the scattered radiation from the cluster/surface system. The cluster-based cross-sections, on the other hand, can be viewed as the quantities which naturally fall out of the conservation-of-energy properties of Eq. (39). To demonstrate this, Eq. (39) is multiplied throughout by a_μ^{j*}, and the result is summed over μ and j. By making use of the properties of the translation matrices, and by introducing the single-origin expansion of the scattered field, the following result is obtained:

$$-\sum_{j=1}^{N_{\mathrm{S}}}\sum_{\mu}\mathrm{Re}\left(1+\frac{1}{\overline{a}_\mu^j}\right)|a_\mu^j|^2 + \sum_\mu |a_\mu|^2 + \mathrm{Re}\sum_{j,i=1}^{N_{\mathrm{S}}}\sum_{\mu,\nu} a_\mu^{j*} R_{\mu\nu}^{j-i} a_\nu^i = -\mathrm{Re}\sum_\mu a_\mu (p_\mu + g_\mu)^*. \tag{63}$$

When multiplied throughout by π/k^2, the first term on the left-hand side corresponds to the absorption cross-section $C_{\mathrm{abs,C}}$ of the cluster—which is the sum of the absorption cross-sections of the individual spheres. The second and the third terms on the left represent the scattering cross-sections based on the direct scattered flux ($C_{\mathrm{sca,C},d}$) and the interference between the direct and the reflected scattered fields ($C_{\mathrm{sca,C},r}$), with the total scattering cross-section $C_{\mathrm{sca,C}}$ being the sum of the two parts. And the two parts of the right-hand side correspond to extinction cross-sections for the direct ($C_{\mathrm{ext,C},d}$) and the reflected ($C_{\mathrm{ext,C},r}$) incident fields.

Of these quantities, the cluster absorption cross-section has the most relevance with respect to the observable properties of the cluster/surface system, in that the energy absorbed by the cluster would be $I_0 C_{\mathrm{abs,C}}$. Likewise, $I_0 C_{\mathrm{sca,C}}$ is the total energy scattered in all the directions by the cluster, yet only a fraction of this energy will be directed away from the surface. Accordingly, $C_{\mathrm{sca,S}} \leqslant C_{\mathrm{sca,C}}$, with the equality holding for a perfectly reflecting surface.

By using the formulas for the incident field coefficients (Eqs. (4) and (11)) and the amplitude matrix (Eq. (51)), it turns out that the surface and the cluster extinction cross-sections are related by

$$C_{\mathrm{ext,S}} = |r(\cos\beta_r)|^2 C_{\mathrm{ext,C},d} + C_{\mathrm{ext,C},r} \tag{64}$$

in which r is the Fresnel reflection coefficient evaluated for the particular polarization state (parallel or perpendicular) of the incident field. This relation has a simple interpretation, in that $I_0 C_{\mathrm{ext,C},d}$ represents the energy removed from the direct incident beam due to absorption and scattering by the cluster. A fraction

$|r(\cos\beta_r)|^2$ of this energy is removed from the reflected beam via surface reflection. In addition, the cluster also removes, via absorption and scattering, $I_0 C_{\mathrm{ext,C},r}$ from the reflected beam.

3. Results and discussion

Codes for implementing the formulation were developed in *Mathematica* and in Fortran-77; the former was used to test the veracity of the various elements of the solution, whereas the latter was to produce an optimized computational procedure. The codes were run on a standard, MS-windows desktop PC.

The sphere cluster/surface scattering problem suffers from what may be called a crowded parameter space. That is, there are a relatively large number of variables which affect the optical properties (sphere size parameters, refractive indices, positions, surface refractive index, angle of incidence) and an equally large number of computable quantities to examine (cross-sections based on surface or sphere formulations, scattering matrix elements as a function of scattering direction). Obviously, a comprehensive investigation of the effects of the variables on the observables is beyond the scope of this paper. In this respect, the calculation results that are provided is meant only as a rough sample that is intended to illustrate some of the interesting features that arise from interactive sphere–surface scattering.

A key item which deserves examination is the accuracy of the NIA, especially when applied to the clusters of spheres lying on a surface. Some indication of how this approximation fares is given in Figs. 2–4, which show the surface extinction and the absorption efficiencies vs. the incidence angle β_r for single, two, and four spheres that have size parameters of either one or 10. The sphere clusters are straight touching chains, and the axis of the chain and the incident direction are in the same plane. Values of the optical constants for the spheres and the surface are the same as those used in Ref. [5], which correspond to polystyrene spheres ($m_S = 1.59 + 0\mathrm{i}$) lying on a silicon surface ($m_b = 3.88 + 0.02\mathrm{i}$). Efficiency factors are defined as the cross-section divided by the projected area $N_S \pi a^2$, and the results are shown for parallel and perpendicular polarization of the incident field.

Even for the 'largest' computational case in this set—that being the four-sphere chain with $x_S = 10$—calculation of the exact solution does not require a long computer run. For this case the individual sphere expansions were truncated at $N_O = 15$ orders, and calculation of all the 4×4 submatrices of the reflection matrix R^{i-j} from Eq. (31) required around 20 s on the PC. Solution of the interaction equations, which was performed iteratively using a biconjugate gradient method, required around 10 s for each incident angle.

Overall, the results indicate that the efficiency factors calculated from the NIA match reasonably the exact values. The difference between the two formulations is largest for the four-sphere chain, yet is also relatively

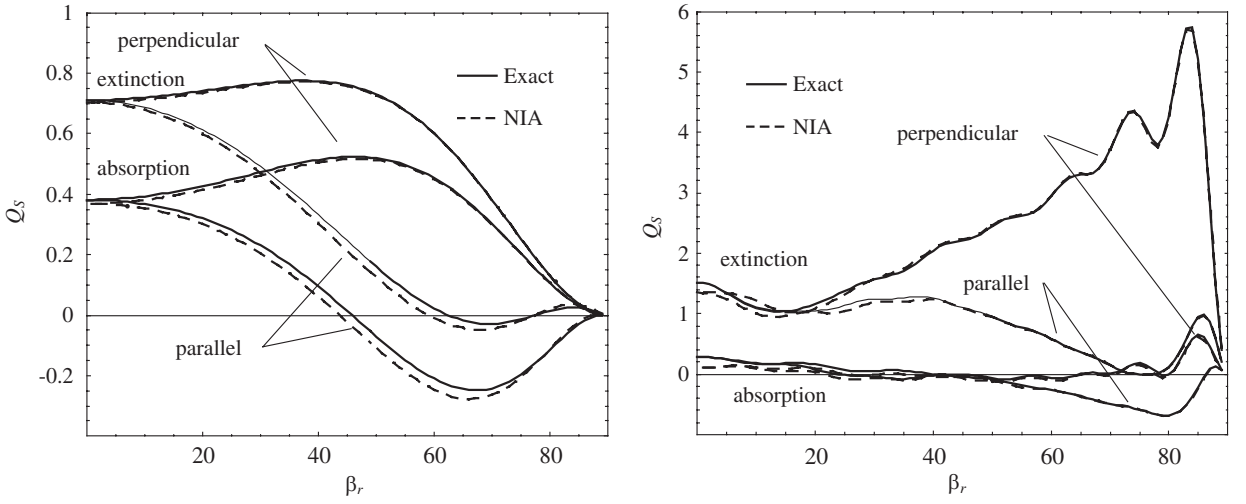

Fig. 2. The surface extinction and the absorption efficiencies vs. the reflection angle for a single sphere. Sphere size parameter $x_S = 1$ (left) and 10 (right).

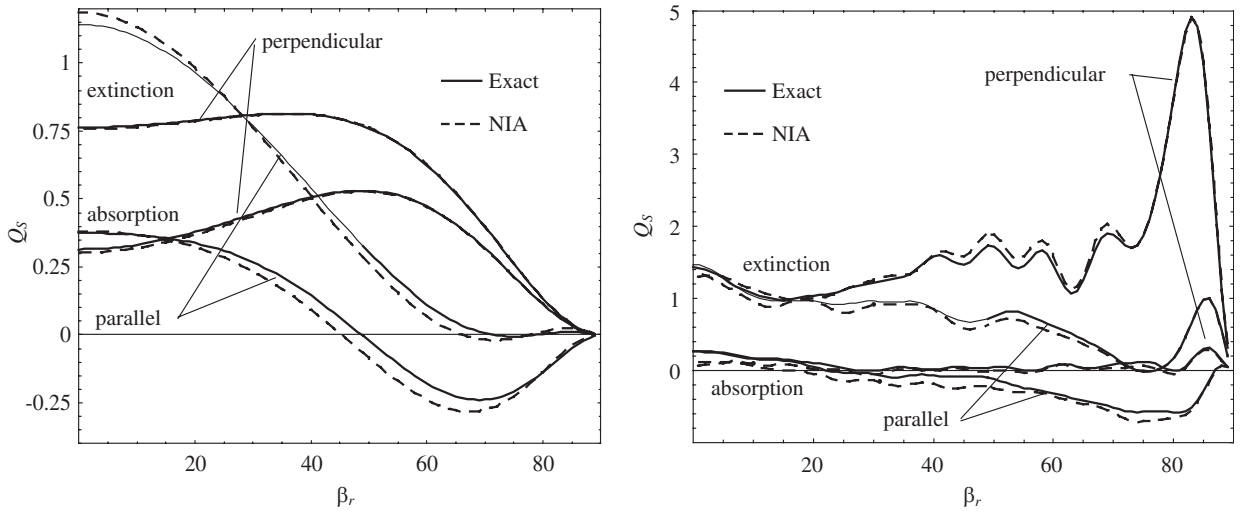

Fig. 3. The surface extinction and the absorption efficiencies vs. the reflection angle for two spheres. Sphere size parameter $x_S = 1$ (left) and 10 (right).

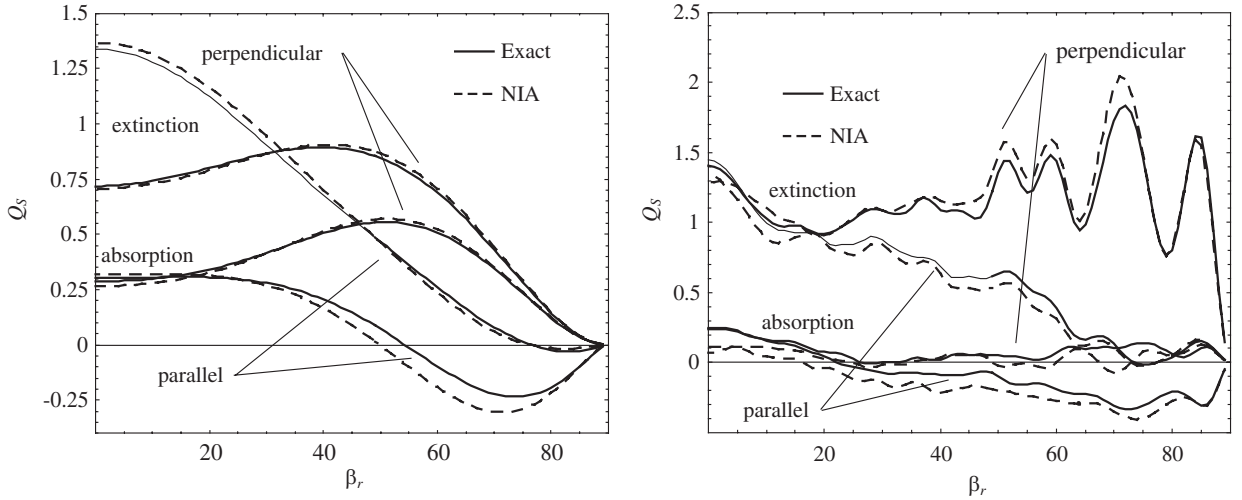

Fig. 4. The surface extinction and the absorption efficiencies vs. the reflection angle for a straight chain of four spheres. Sphere size parameter $x_S = 1$ (left) and 10 (right).

similar for the two size parameters. The effect due to the elongation of the particle is to be expected; forward-scattered radiation from the spheres nearest to the incident source reflects and interacts with spheres farthest from the source. The reflection angles that characterize this interaction are relatively large, and accordingly the Fresnel coefficients that modify the interaction will not be equal to the normal incidence values. Wriedt and Doicu reached a similar conclusion when examining the surface interactions by elongated ellipsoidal particles [5].

As would be gathered from Eq. (58), the extinction efficiency curves display behavior that has features of both the sphere scattering and the surface reflection. The Brewster angle for the nonabsorbing silicon with $m_b = 3.88$ is 76°, and, as expected, the extinction efficiency for parallel incident polarization becomes small near this angle. An interesting phenomenon, seen for the $x_S = 1$ results at angles slightly smaller than the Brewster angle, is the negative value of extinction for parallel polarization. Such a behavior implies that scattering from the particle has the net effect of adding energy to the reflected plane wave. Unfortunately, this is not due to some exotic, previously unrecognized mechanism for negative absorption or scattering; rather,

the effect is simply an outcome of the surface extinction definition used herein, i.e., the interference of the scattered field with the reflected plane wave. The scattered field arises from the scattering of the incoming (direct) and the reflected plane wave. For both the incident and the scattering angles near the Brewster angle, the latter component will be small as will be the amplitude of the reflected plane wave. The former component, however, will depend almost entirely on the scattering characteristics of the spheres. Depending on these characteristics, the amplitude and the phase of the scattered field in the direction $\theta = \beta_r$ could constructively interfere with the reflected plane wave, thus leading to a negative extinction.

The surface absorption plots for the $x_S = 1$ case all show similar trends—which depend strongly on the polarization state of the incident field—for all three cluster configurations. For parallel polarization the surface absorption becomes negative for the reflection angles greater than around 45°, whereas the surface absorption for the perpendicular polarization is positive throughout all the angles. As discussed in the previous section, the positive and the negative surface absorption implies that the net effect of the sphere(s) is to decrease and increase, respectively, the reflectivity of the surface. As was the case with negative extinction, the negative absorptivity occurs in regions near the Brewster angle where the surface reflectivity is low, and results from the effect of scattering of the direct incident field by the spheres into directions away from the surface. The net effect of the spheres on the surface would therefore be to reduce the polarizing effects of surface reflection near the Brewster angles, i.e., for unpolarized incident radiation, the spheres would increase the effective parallel polarized reflectivity and decrease the perpendicular reflectivity.

At near-normal incidence, a noticeable effect of cluster configuration for the $x_S = 1$ case is the difference between the parallel and the perpendicular extinction and, to a lesser extent, the absorption efficiencies for the $N_S = 2$ and 4 chains. For the particular orientation of the sphere chains, parallel incident polarization results in the incident electric field parallel to the chain axis, and such a state—for spheres with relatively small size parameters—enhances the field coupling among the spheres. Similar effects are observed for the isolated clusters of spheres [12].

In contrast, the results for the $x_S = 10$ case show a significant effect of the chain length at relatively large incident angles. For the single sphere, zero extinction and negative absorption is observed for parallel incident polarization near the Brewster angle—as is the case with $x_S = 1$—yet the perpendicular extinction shows a strong peak at near-grazing incidence angles. The perpendicular Fresnel coefficient is near unity at these angles, and this can result in a strong coupling of the direct and the reflected components of the forward-scattered field for θ slightly less than 90°. Indeed, the peak value of the perpendicular surface extinction for the single sphere, $x_S = 10$ case, is around twice that of the isolated sphere extinction efficiency of 2.6, which indicates a direct addition of the direct and the reflected scattered field into the forward direction. A similar enhancement of the perpendicular extinction is observed for the $N_S = 2$ case, although the peak has become much more compressed around a smaller range of incident angles. And for $N_S = 4$ the enhancement has been washed out by the ripple structure.

Attention is now turned to the distribution and polarization characteristics of the scattered radiation from the clusters. Shown in Figs. 5–7 are the values of S_{11} and S_{12}/S_{11} vs. scattering angle θ, calculated using the exact and the NIA models, for the three cluster configurations used in the previous plots (single, double, and four sphere), and for $x_S = 10$ and normal incidence. Refractive index values are the same as before. The scattering plane is defined by $\phi = 0$, i.e., in the direction of the cluster axis. The S_{11} element is scaled by $N_S \pi a^2$ so that it integrates over the hemisphere to $Q_{sca,S}$.

As was the case with the efficiency factors, the NIA becomes less accurate in predicting the distribution of S_{11} as the number of spheres in the cluster increases. In general, the approximation represents well the backscattering peak in intensity for all three sphere cluster configurations, yet deviates appreciably from the exact results for larger scattering angles. This behavior is even more apparent in the results for the polarization ratio S_{21}/S_{11}. Again, the behavior near backscattering is well represented by the NIA, yet the predictions diverge considerably at larger scattering angles.

An indication of the scattering patterns produced by the off-normal incident radiation is given in Figs. 8 and 9. Shown are color contour plots for S_{11} and S_{12}/S_{11} for the two cluster configurations of a four-sphere straight chain and a four-sphere tetrahedral cluster. The chain is aligned along the x-axis, as before, and the tetrahedron has three of the spheres in contact with the surface and a pair of these three parallel to the x-axis. Sphere size parameters are $x_S = 10$ for both the sets, and the refractive index values are the same as before.

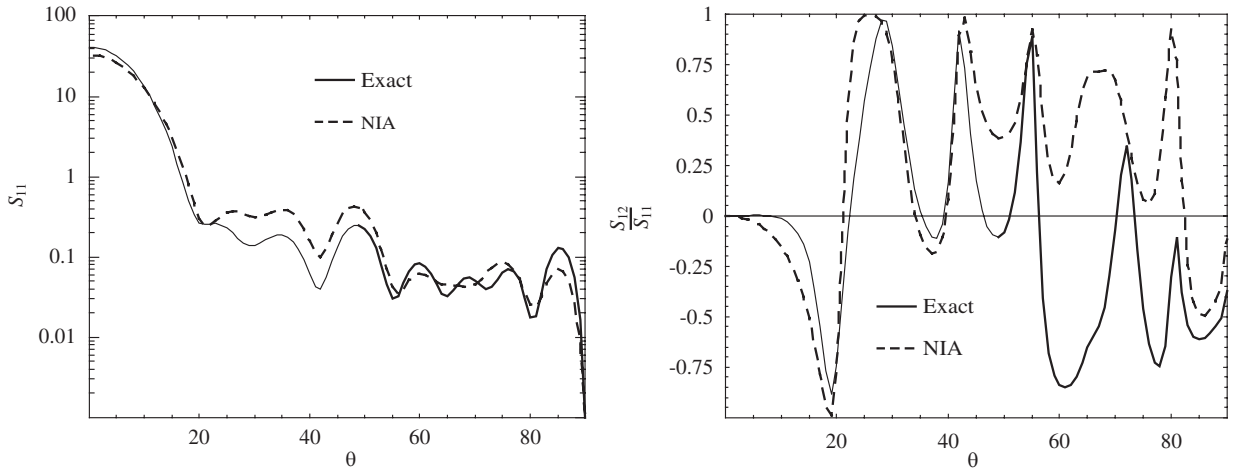

Fig. 5. The scattering phase function S_{11} and the polarization ratio S_{12}/S_{11} vs. the scattering angle θ for a single sphere. Sphere size parameter $x_S = 10$, normal incidence.

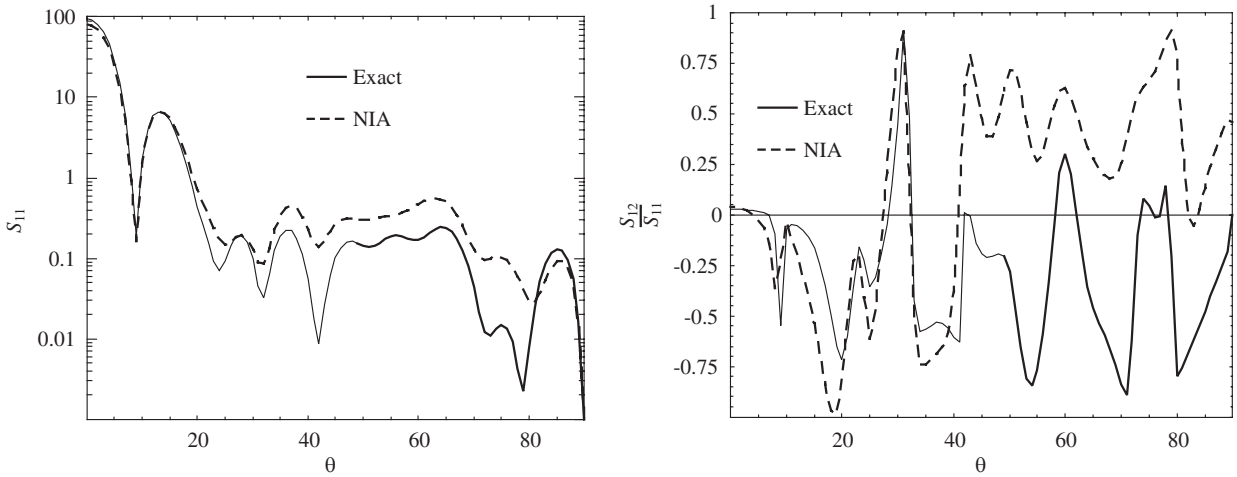

Fig. 6. The scattering phase function S_{11} and the polarization ratio S_{12}/S_{11} vs. the scattering angle θ for two spheres in contact. Sphere size parameter $x_S = 10$, normal incidence.

Incident radiation is characterized by $\beta_r = 20^\circ$ and $\alpha_r = 45^\circ$; these values were chosen explicitly so that the incident propagation direction was not parallel or perpendicular to an axis or plane of symmetry of the cluster. The contour plots show a 2-D rectangular projection of the scattering pattern centered about the normal direction, with the opposite corners of the plots corresponding to $\phi,\ \theta = -135^\circ, 45^\circ$ and $\phi, \theta = 45^\circ, 45^\circ$. Note that the horizontal and the vertical edges of the plots are parallel to the x and y directions of the target frame. Results are given for the exact and the NIA.

For both the cluster configurations, the S_{11} plots show the strong reflection (or forward-scattering) peak at $\theta = \beta_r = 20^\circ$ and $\phi = \alpha_r = 45^\circ$, and a smaller backscattering peak at $\theta = \beta_r = 20^\circ$, $\phi = \alpha_r - \pi = -135^\circ$. Aside from this, the two configurations produce distinctly different patterns. The straight chain produces, via interference, a ring-like structure (i.e., vertical lines), which is due to the axial symmetry of the cluster. On the other hand, little organized structure is evident in the tetrahedron S_{11} distribution, except perhaps the three-lobed pattern centered about the forward-scattering lobe. Another item to note is that, for the S_{11} patterns, the

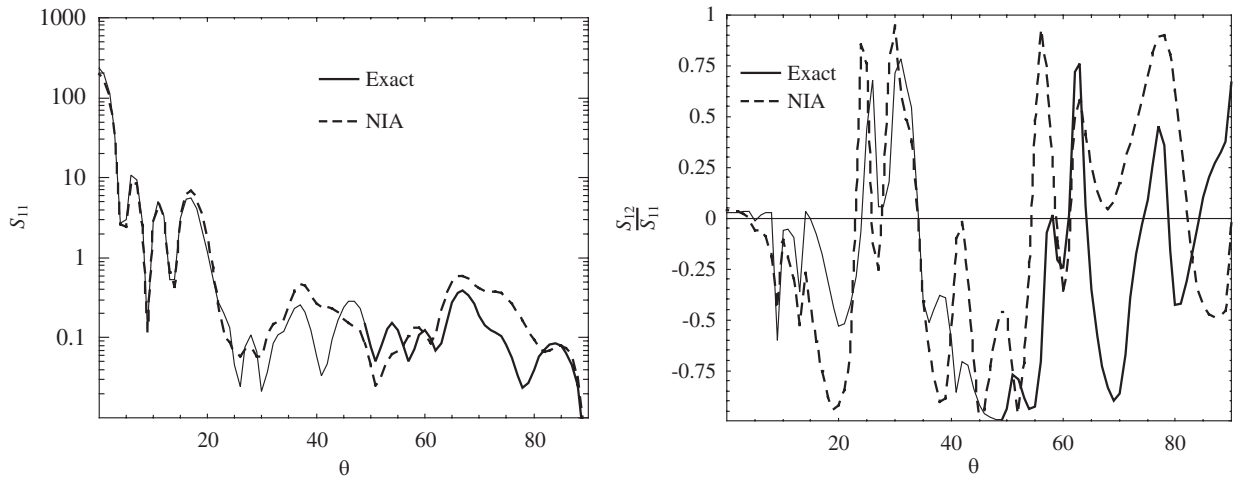

Fig. 7. The scattering phase function S_{11} and the polarization ratio S_{12}/S_{11} vs. the scattering angle θ for a straight chain of four spheres. Sphere size parameter $x_S = 10$, normal incidence.

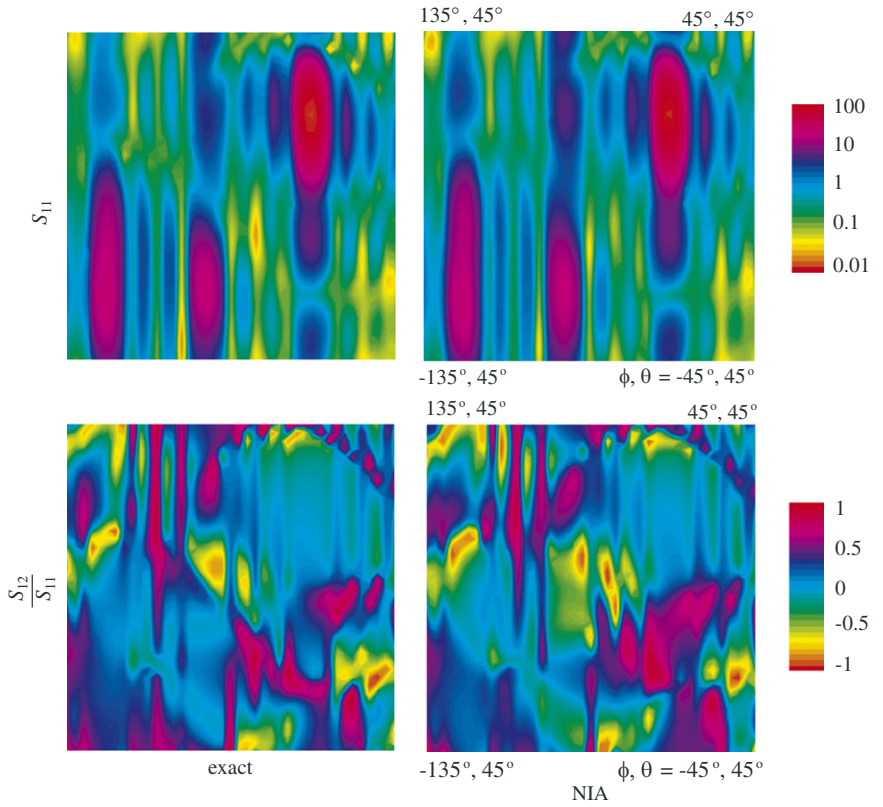

Fig. 8. The contour plots of the scattering phase function S_{11} (top) and the polarization ratio S_{12}/S_{11} (bottom) for a straight chain of four spheres. Sphere size parameter $x_S = 10$, reflection direction $\beta_r = 20°$, $\alpha_r = 45°$.

exact and the NIA methods are very much in line for both the clusters; small differences in magnitude are discernable yet the overall structure is well mapped by the NIA.

Similar cluster-dependent structure—or lack thereof—is observed in the polarization ratio. Both types of clusters show a region of zero polarization ratio about the forward-scattering direction, and the line patterns

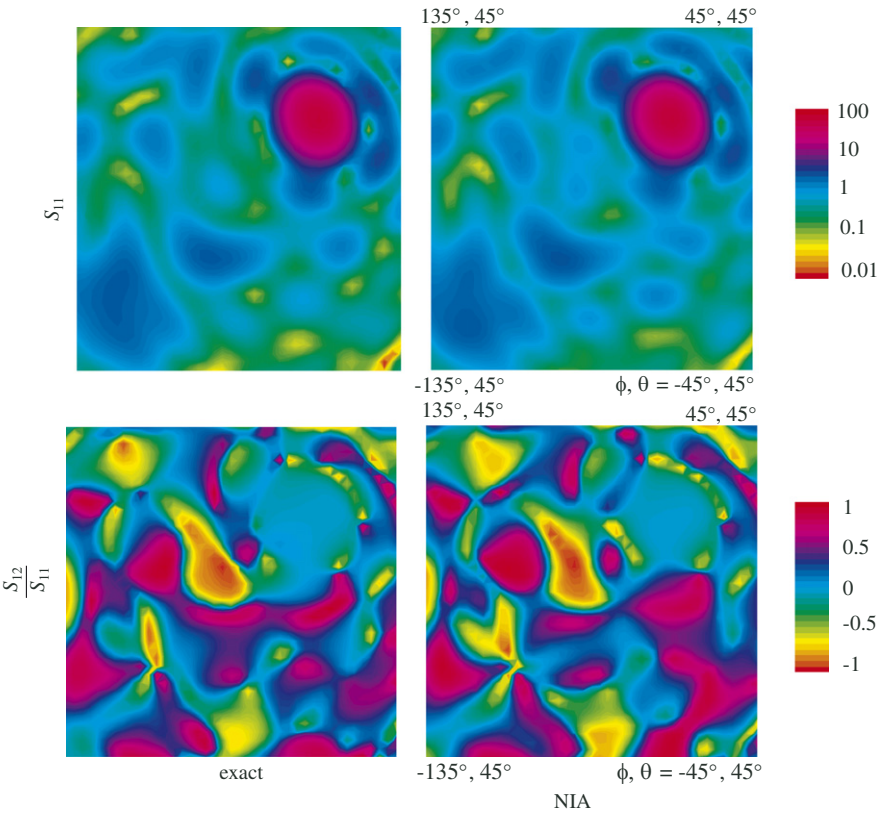

Fig. 9. The contour plots of the scattering phase function S_{11} (top) and the polarization ratio S_{12}/S_{11} (bottom) for a tetrahedral cluster of four spheres. Sphere size parameter $x_S = 10$, reflection direction $\beta_r = 20^\circ$, $\alpha_r = 45^\circ$.

due to the chain symmetry are again visible. As was the case with Figs. 5–7, differences between the exact and the NIA methods are much more evident in the depolarization ratio results.

4. Conclusions

The intention of this work has not been to comprehensively examine the scattering and absorption features of sphere clusters on surfaces. Rather, the objective has been to develop a formulation and a code which will make tractable the exact calculation of such features. Even though the NIA works reasonably well in many conditions for many properties, it has been shown that parameter space exists in which the discrepancies between the NIA and the exact formulations are considerable. Except in conditions where the NIA formulation is known to hold in a limiting sense, such as a perfectly reflecting surface or clusters that are relatively far removed from the surface, it is difficult to predict *a priori* the accuracy of the approximation.

In some respects and for some conditions, the NIA can offer a significant computational advantage. The translation matrix in Eq. (34) can be factored into rotational and axial translation parts, and by doing so the matrix–vector multiplication process can be made faster and the memory requirements lower [11]. The exact reflection matrix, on the other hand, does not appear to offer this factorization potential. In addition, the NIA can be used to generate an outgoing VWH expansion for the scattered and reflected field that is convergent at all the points above the surface. In contrast, the exact, regular VWH expansion of the field has a limited radius of convergence; this does not pose a problem as far as the solution of the interaction equations is concerned, yet it could be problematic in terms of calculating the exterior field in the near-field neighborhood of the spheres and the surface.

The above points aside, a reason for using the NIA should not be the computational complexity of the exact method. Indeed, the exact computation of the surface reflection matrix poses little extra computational burden on the overall calculation procedure, a procedure in which, it should be emphasized, the dominant computational effort typically involves the numerical solution of the interaction equations.

Acknowledgments

The author wishes to thank Pinar Menguc, Michael Mishchenko, Gorden Videen, and Thomas Wriedt for helpful advice during the preparation of this paper.

Appendix A

A.1. Vector spherical harmonics

The VSH functions used in this work are defined by

$$\mathbf{N}^{(v)}_{mn2}(\mathbf{r}) = \left(\frac{2n+1}{4n(n+1)}\right)^{1/2} \nabla \times \left(\mathbf{r}\psi^{(v)}_{mn}(\mathbf{r})\right), \tag{65}$$

$$\mathbf{N}^{(v)}_{mn1}(\mathbf{r}) = \frac{1}{k}\nabla \times \mathbf{N}^{(v)}_{mn2}(\mathbf{r}), \tag{66}$$

where

$$\psi^{(v)}_{mn}(\mathbf{r}) = \begin{cases} \left(\dfrac{(n-m)!}{(n+m)!}\right)^{1/2} j_n(kr)P^m_n(\cos\theta)\mathrm{e}^{\mathrm{i}m\phi} & v=1, \\ \left(\dfrac{(n-m)!}{(n+m)!}\right)^{1/2} h_n(kr)P^m_n(\cos\theta)\mathrm{e}^{\mathrm{i}m\phi} & v=3. \end{cases} \tag{67}$$

A.2. Generalized spherical functions

The spherical functions $\mathscr{D}^{(n)}_{km}(\cos\theta)$, which appear in Eq. (30), are given by

$$\mathscr{D}^{(n)}_{km}(\cos\theta) = (-1)^{m+k}\left[\frac{(n+m)!(n-m)!}{(n+k)!(n-k)!}\right]^{1/2}\left[\frac{1+\cos\theta}{2}\right]^{(m+k)/2}\left[\frac{1-\cos\theta}{2}\right]^{(m-k)/2} P^{(m-k,m+k)}_{n-m}(\cos\theta) \tag{68}$$

with $P^{(m-k,m+k)}_{n-m}(\cos\theta)$ representing the Jacobi Polynomial. Special cases are

$$\mathscr{D}^{(n)}_{km}(x) = \mathscr{D}^{(n)}_{-m-k}(x) = (-1)^{m+k}\mathscr{D}^{(n)}_{-k-m}(x), \tag{69}$$

$$\mathscr{D}^{(n)}_{0m}(x) = \left(\frac{(n-m)!}{(n+m)!}\right)^{1/2} P^m_n(x). \tag{70}$$

A.3. Translation matrix

Elements for the translation matrix $J^{j-i}_{mnp\,klq}$ are given by

$$J^{i-j}_{mnp\,klq} = -(-1)^m[(2n+1)(2l+1)]^{1/2} i^{n-l}\sum_w \mathrm{i}^w C^w_{-mn,kl} C^w_{-1n,1l}\psi^{(1)}_{k-mw}(\mathbf{r}_{i-j}) \tag{71}$$

in which $\mathbf{r}_{i-j}$ is the position vector of origin i relative to origin j. The order w in the sum takes on the values of $w = |n-l|, |n-l|+2, \ldots n+l$ when $p=q$, and $w = |n+l|+1, |n-l|+3, \ldots n+l-1$ when $p \neq q$. The formula for H^{i-j} is the same, with $\psi^{(1)}$ replaced by $\psi^{(3)}$.

References

[1] Bobbert PA, Vlieger J. Light scattering by a sphere on a substrate. Physica 1986;137A:209–42.
[2] Videen G. Light scattering from a sphere on or near a surface. J Opt Soc Am A 1991;8:483–9 errata: J Opt Soc Am A 1992; 9:844–5.
[3] Videen G, Turner MG, Iafelice VJ, Bickel WS, Wolfe WL. Scattering from a small sphere near a surface. J Opt Soc Am A 1993;10:118–26.
[4] Fucile E, Denti P, Borghese F, Saija R, Sindoni OI. Optical properties of a sphere in the vicinity of a plane surface. J Opt Soc Am A 1997;14:1505–14.
[5] Wriedt T, Doicu A. Light scattering from a particle on or near a surface. Opt Commun 1998;152:376–84.
[6] Wojcik GL, Vaughan DK, Galbraith LK. Calculation of light scatter from structures on silicon surfaces. In: Batchelder JS, Ehrlich DJ, Tsao JY, editors. Lasers in microlithography, vol. 774. Proceedings of the society of photo-optical instrumentation engineers 1987. p. 21–31 [chapter 6].
[7] Johnson BR. Calculation of light scattering from a spherical particle on a surface by the multipole expansion method. J Opt Soc Am A 1996;13:326–37.
[8] Denti P, Borghese F, Saija R, Fucile E, Sindoni OI. Optical properties of aggregated spheres in the vicinity of a plane surface. Appl Opt 1999;16:167–75.
[9] Bohren CF, Huffman DR. Absorption and scattering of light by small particles. New York: Wiley; 1983.
[10] Press WH, Flannery BP, Teukolsky SA, Vetterling WT. Numerical recipes. Cambridge: Cambridge University Press; 1986.
[11] Fuller KA, Mackowski DW. Electromagnetic scattering by compounded spherical particles. In: Mishchenko MI, Hovenier JW, Travis LD, editors. Light scattering by nonspherical particles: theory, measurements, and applications. New York: Academic Press; 2000 [chapter 8].
[12] Mackowski DW. A simplified model to predict the effects of aggregation on the absorption properties of soot particles. JQSRT 2006;100:237–49.